Correlation between Numerical and Experimental Structural Resistance of a Safety Relevant Aluminum Automotive Component

Silvia Cecchel [1,2,*], Davide Ferrario [1], Francesco Mega [1] and Giovanna Cornacchia [2]

[1] Streparava SpA, Via Zocco 13, 25030 Adro (BS), Italy

[2] Department of Industrial and Mechanical Engineering (DIMI), University of Brescia, via Branze 38, 25123 Brescia, Italy

[*] Correspondence:s.cecchel@streparava.com

Abstract: Accurate implementation of weight reduction for the development of innovative safety-relevant components, such as suspension assemblies, requires a careful evaluation of the structural resistance. The validation of these critical parts usually employs Finite Element Analysis (FEA) during the design phase and laboratory tests on prototypes during later stages. However, the results of these established methods have rarely been numerically compared. The present paper introduces a method for comparing FEA and testing, based on the elaboration of micro-strains acquired with strain gauges positioned in specific regions. The model was applied to the real case study of an innovative lightweight cross beam. FEA simulations and bench tests under different conditions that were representative of the operating environments were carried out. Two different relevant configurations of fatigue bench tests were considered. Then, the data obtained from testing were numerically elaborated in order to compare them with the analytical results. Real data from in-field measurements were used. The cross beam endured at the elevate mission loads reproduced at the bench test. The FEA and testing results were aligned. The correlation method was proven to be reliable, since it made it possible not only to numerically evaluate the testing output, but also to validate the calculation tools, and it could be extended to similar applications in future.

1. Introduction

The weight reduction of automotive components, as is well-known, is one of the most feasible measures for reducing vehicle emissions [1–5]. It is commonly applied in the production of new cars and high-performance vehicles, although it has only recently been approached for heavier means of transport [6,7]. The difficulty arising from the substitution of traditional metals (i.e., steel, cast iron) with lighter ones (i.e., aluminium alloys) in this class of vehicles is related both to the elevated operating loads, which imposes strict requirements on resistance and stiffness, and to the lower eligible costs. Of course, the preservation of the safety and performance levels required by automotive standards is a very important aspect [8,9] that needs to be carefully evaluated when reducing component weights. This is particularly true for safety-critical parts such as the suspension cross beam, control arms, and brakes, failures in which result immediately in the loss of vehicle orientation [10]. Starting from this definition, it is clear that the structural resistance of these products is a very relevant and challenging task. Therefore, their development and validation process comprises different forms of analysis, considering the several factors affecting the mechanical behaviour (i.e., the design, material, production technology, process parameters, etc.), the results of

which lead to the final determination of the component features. Firstly, Finite Element Analysis (FEA) is a fundamental tool in the evaluation of structural performance, and is used in order to drive the design to more mature levels prior to the availability of a prototype [11]. The main advantages of the preliminary optimization of a design include: saving the cost of physical prototyping at an inappropriate point in time, lowering the development time and the time to market, and further reducing the component weight thanks to geometrical optimization. The potential risks and failure modes can be predicted and prevented much earlier in the development stage thanks to virtual analysis [11]. Similarly, when working on new applications, it may be necessary for some laboratory tests (e.g., tensile tests, corrosion analysis, microstructural investigation, etc.) to preliminarily evaluate some sample properties far ahead of a prototype's availability, and to consequently set the features of the components [7]. These tests could be also useful for improving the precision of the FEA model through the implementation of more detailed properties related to the case studied. Once the design and properties of the components have been defined, prototypes can be subsequently be produced and validated.

Physical durability tests for validation purposes are usually carried out on protypes at later stages of the development process. The final aim of such testing is to confirm that the physical components meet the expected mechanical resistance suggested by the initial numerical computer simulations [12]. Indeed, for many safety-critical issues, physical testing remains indispensable. Field testing is the most natural durability assessment procedure for demonstrating the reliability of a vehicle with respect to chassis and suspension endurance. This consists of driving along a predefined path that reflects different public road conditions (e.g., highway, urban, hill). However, vehicle road tests are very time consuming, expensive, generally difficult to reproduce, and are usually impossible to carry out in the early development stages [13–16]. A widely employed option for accelerating the process of durability analysis is indoor testing trough test rigs that have been designed for this purpose. In addition to the reduction in testing time, there are other benefits, including no full vehicle prototype being required for the validation of the component or subsystem, while the tests are simultaneously more readily reproducible, and the experiments can be much more easily observed [13].

In the particular case of suspensions, tests are usually performed on specially designed benches employed to investigate the fatigue behaviour of axle systems under various driving and road conditions. These tests are carried out with equivalent loads. Specifically, mission profiles consist of several loading events that are representative of service loads generated during vehicle circulation. The real loads (forces and moments) transmitted to the wheel during the vehicle mission are measured with Wheel Force Transducers (WFT) and elaborated into reduced time histories. During road simulator testing, these time histories are applied to systems by means of movements on the wheels while the axle is attached to fixed blocks [7]. Road simulator test rigs are commonly used for subsystems of different sizes [13].

Specific loading conditions are sometimes not suitable for testing by means of a road simulator test bench. This could be attributable to either the difficulty of sourcing all the elements of an elaborate subsystem for the testing of a single component (e.g., subsystem = full suspension; single component = cross beam) or to the particular need to investigate the effect of external actions in specific areas of the part. Indeed, tests on subsystems or individual chassis components are usually performed on smaller test rigs, which have the advantage of also being more affordable. For the sake of clarity, an example of this test is the evaluation of cross beam fatigue resistance under the condition of the loads transmitted by the steering system.

Beyond the scope of initial component testing (final design validation), a second interesting purpose could involve a more cooperative usage of numerical and laboratory rig simulation. Indeed, test and analysis correlation is an emerging field in today's automotive industry [12] that aims to evaluate the reliability of finite element models based on the results of tests carried out using the modelled structure. It is worthwhile noting the relevance of such verification for safety-critical components, which require reliable and very precise simulations. However, this kind of correlation has only rarely been investigated in relation to suspension durability tests. Indeed, even if, in the

literature, many correlations of calculations and tests can be found related to a number of different applications, to the best of the authors' knowledge, none of these numerically compare the output of suspension component bench tests with the values calculated on the basis of simulations. Specifically, testing results are usually analysed in a qualitative way; the absence of cracks—or their limited degree of extension, depending on the specific application and the relative standard—is typically the only parameter employed for the validation of the test. In line with these considerations, the relevance of the method introduced in the present work is clear, as it presents a more complete way of analysing the output of the suspension durability test.

For the sake of clarity, the subject of this article belongs to the wider research on the reduction of the weight of safety-relevant structures in the Commercial Vehicle (CV) field [17–24]. This project developed a new concept for aluminium cross beam suspensions in CV as a replacement for the currently used steel components. The related advantages include the affordability of the achieved solution, a weight reduction of about 50%, environmental benefits, avoidance of painting, and excellent recyclability. The use of appropriate materials, a new design concept, and a careful function integration allowed the structural limits to be overcome. The feasibility of this solution was verified on the basis of detailed characterization and testing, which consisted of an analysis of the most relevant failure modes, along with a complete mechanical and microstructural characterization. In particular, microstructure analysis, hardness tests, tensile tests, fractography, salt spray test, and fatigue test were conducted in a bench road simulation.

The present paper introduces a method for deeply investigating the structural resistance of new components. The model was applied for the case of the real cross beam introduced above. The research focused on the numerical elaboration of the data coming from the final validation of the innovative cross member in order to draw a correlation between these empirical results and the analytical ones. As already stated, few works could be found investigating this activity, and the results could be potentially extended to future applications of this complex product validation.

In particular, this research reports the structural simulations used for both the virtual validation of the cross member and the selection of the most appropriate features for its final configuration (design, material, technology). Then, the paper shows the results of: (i) the fatigue test bench road simulation conducted with time histories developed with reference to actual missions; and (ii) fatigue testing under hydraulic steering system loads performed on a smaller test bench. Subsequently, the model object of the research was applied in order to find a numerical comparison between the FEA and testing results.

Finally, after the test, the component was analysed by means of liquid penetrant testing and a microstructural investigation of the tested prototypes in order to confirm the absence of cracks related to the endurance tests.

It is important to highlight that the present activity is conducted on the basis of many actual data obtained from experimental tests (e.g., mission profiles and mechanical properties of components) in order to guarantee that the results are as accurate and reliable as possible. This is of great relevance, both for the validation of safety-relevant components and for unusual correlations between road simulations and FEA results.

2. Materials and Methods

2.1. Geometry, Materials and Process Description

As stated in the introduction, the front cross beam is a safety-critical component, usually made of heavy metals, that constitutes a link between the suspension elements, the steering knuckles and the main frame of the vehicle. During this project, weight reduction of the cross beam was achieved using High Pressure Die Casting (HPDC) technology with the aluminium alloy EN AC 43500. In order to endure the elevated loads typical of CV applications, the component was completely re-designed. The final design comprised a hollowed structure guaranteeing a higher stiffness in comparison to the traditional open sections. Complex and extended metal cores were used to achieve this innovative shape. Figure 1 represents the component and the main areas connected with the

other suspension elements (highlighted in red colour). The cross beam dimensions are about 1260 mm × 450 mm × 260 mm, with an average thickness of 4 mm and a weight of 15 kg, thus representing a weight reduction of about 50% in comparison with currently produced steel components. An ITALPRESSE TF cold chamber machine (ITALPRESSE, Brescia, Italy) with a maximum locking force of 3000 t equipped with Fondarex vacuum was used to produce the suspension cross beam prototypes. More details about the component properties can be found in the previous works of the authors [17–24].

Figure 1. Cross beam design and the main areas connected with the other suspension elements (highlighted in red colour).

The aluminium alloy used for the production of the cross beam prototypes is EN AC-43500 alloy, the chemical composition of which is reported in Table 1.

Table 1. Chemical composition of EN AC 43,500 aluminium alloy [25].

	Si	Fe	Cu	Mn	Mg	Ni	Zn	Sn	Ti
EN AC-43500	9.5–11.5	0.15	0.03	0.5-0.8	0.1–0.5	-	0.07	-	0.15

The component was tested in the as-cast state (F).

The variability in mechanical resistance was related to the different thickness and the consequent solidification speed of the various areas of this high-dimensional component. Indeed, the mechanical characterization of the prototypes, detailed in [8], was carried out both for samples machined out of the components and on samples cast separately by die casting in different areas in order to evaluate the real properties of the cross beam in detail. At least four measurements were taken for each condition, and the average value is reported for each. The mechanical properties were lower in areas located close to high thickness zones ($\sigma_{p0,2}$ = 117 ± 3 MPa, σ_m = 234 ± 25 MPa, $A\%$ = 6.4 ± 3.8%) than both those calculated for areas distant from these zones ($\sigma_{p0,2}$ = 134 ± 5 MPa, σ_m = 266 ± 20 MPa, $A\%$ = 4.7 ± 1.8%) and for those measured in samples cast separately from the same die ($\sigma_{p0,2}$ = 134 ± 7 MPa, σ_m = 258 ± 5 MPa, $A\%$ = 5 ± 0.9%). More detail regarding the characterization and the results can be found in a previous work of the authors [8]. These data were also in agreement with the nominal range of mechanical properties for this alloy ($\sigma_{p0,2}$ = 120–150 MPa, σ_m = 250–290 MPa, $A\%$ = 5–11%, σ_{FAF} = 89 MPa) [25].

2.2. Experimental and Numerical Setups

The method consists of three steps:

i)   FEA performed with standard load cases is used to verify the structural behaviour of a re-designed component under standard operating conditions. For example, in order to find the lightest geometry that is sufficiently resistant under the operating conditions, these

structural simulations can be used to define a lightweight design, which can be achieved after many iterations of the component shape.

ii)   A selection of physical durability tests is carried out on protypes to confirm that the physical component meets the requirements in terms of mechanical resistance. In this phase, a higher precision can be introduced using real data obtained from experimental investigation of the application (e.g., mission profiles and experimental mechanical properties of components).

iii) Identification of an efficient method to numerically evaluate the testing outputs in order to provide a correlation with the FEA simulation. For example, strain gauges can be introduced in the most representative areas evaluated following FEA examination.

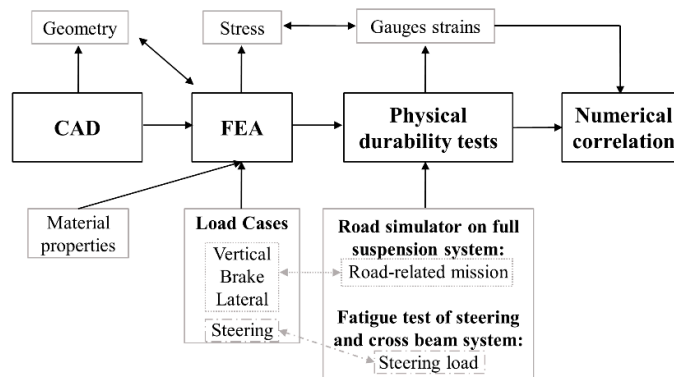Figure 2 shows a flowchart of this method applied for development of a cross beam.

Figure 2. Flowchart of experimental and numerical development of a cross beam suspension.

2.2.1. Finite Element Analysis (FEA)

The structural resistance of the cross beam was evaluated by developing a Multibody simulation (MBS) and an FEA model based on MSC/AdamsCar and MSC Marc/Mentat, respectively.

Firstly, in order to determine the forces of the main load set conditions acting on each component, an elastokinematic multibody model of the entire suspension system was defined and carried out in MSC/AdamsCar. The suspension system modelled was composed not only of the cross beam but also of all the suspension elements connected to it that were located between the steering and the wheels. This made it possible to calculate the forces operating on the cross beam, starting from the load at wheels input. Figure 3 represents the load at wheels input (upper-left side of the picture) and the suspension system model. Letters from A to F indicate kinematic hard points; in particular, A, C, D and F are directly connected with the cross beam.
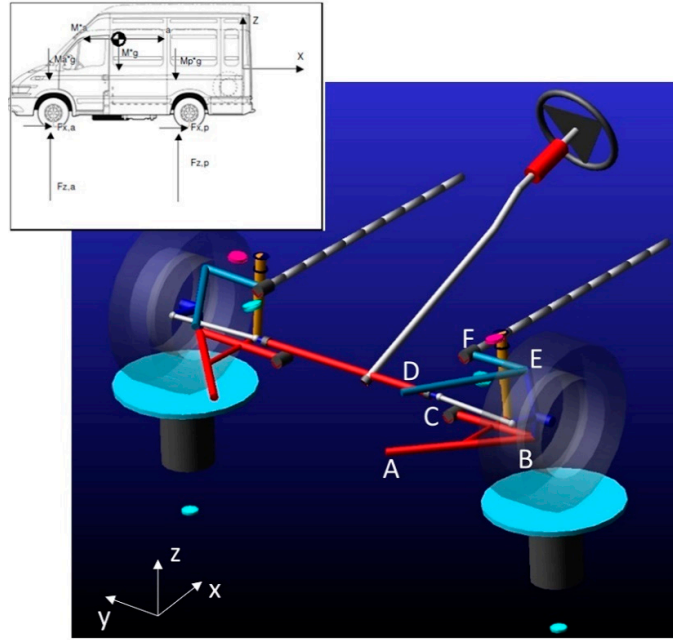
Figure 3. Load at wheels input and MSC/AdamsCar suspension system model.

Three load cases were investigated: vertical load, brake and lateral loading, as reported in Table 2. These have historically proven to be effective for cross beams, and are normally used during the design of this kind of component.

Table 2. Load cases applied in MSC/AdamsCar.

Load Case	Loads at Wheels (kN)		
	X	Y	Z
Vertical	0	0	24.7
Brake	14.19	0	15.7
Lateral	0	14.5	20.6

The model implemented in MSC/AdamsCar calculates the forces at the various cross beam suspension kinematic hard points, which were then used as inputs for the structural FEA on the cross beam performed in MSC Marc/Mentat. The MSC Marc/Mentat model and the hard points (named A, C, D, F as for Figure 3) are reported in Figure 4.
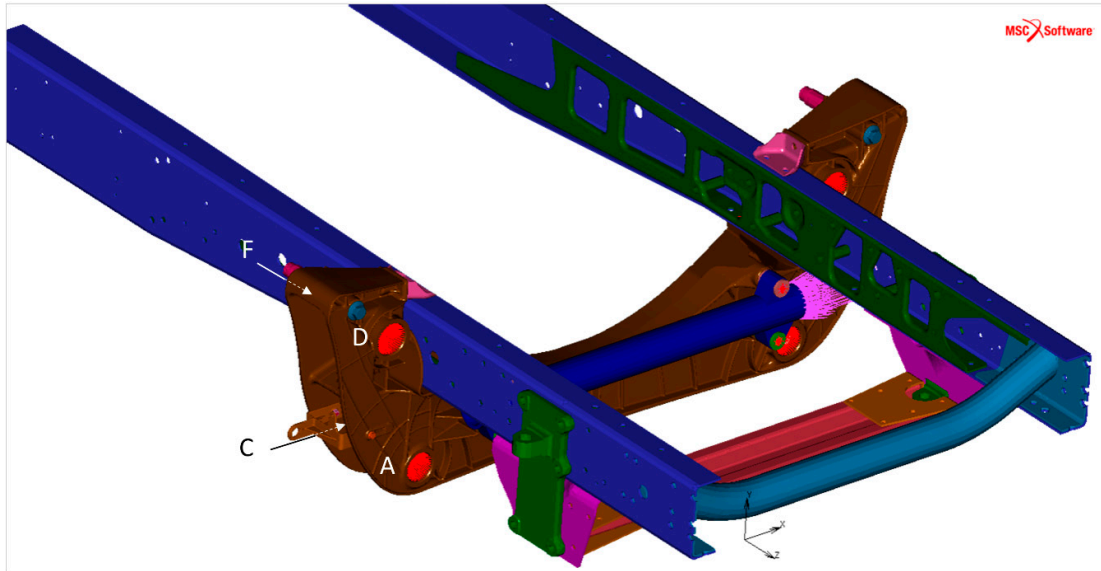
Figure 4. MSC Marc/Mentat model of the cross beam suspension and kinematic hard points.

The MSC Marc/Mentat analysis was focused on cross beam behaviour. The cross member model also included the interfaces with elements typically linked to components on the vehicle (e.g., steering, bushing, frame, screws). The finite element model is composed of about 2.8×10^6 tetrahedral elements and 6.9×10^5 nodes. The cross beam mechanical properties used for the simulation were E = 70 GPa, $\sigma_{p0,2}$ = 120 MPa, σ_m = 250 MPa, $A\%$ = 5%. It can be noted that these values correspond to the lower extreme of the experimental EN AC-43500 range reported in Section 2.1 which were selected in order to be conservative, as is recommended for safety-relevant applications.

The load cases simulated in MSC Marc/Mentat are composed of:

i)   the loads acting on the cross beam due to load at the wheels inputs, as derived from MSC AdamsCar,

ii) a relevant load case related to the steering of a stationary vehicle (F_x = 0 kN, F_y = 29 kN, F_z = 0 kN). This is a misuse condition representing the maximum load transmittable by the steering arms. For this load case, the force was applied based on a realistic representation of the connection between the hydraulic steering system and the cross beam, which were the main components of the subsystem.

The results of these analyses show the stress acting on the component, which was used to finally evaluate the cross beam resistance. The thresholds considered were based on the permissible stress traditionally used and historically proven to be effective for cross beams. In particular, these were set at:

$$\sigma < \sigma_{FAF} \tag{1}$$

$$\sigma < \sigma_{p0,2} \tag{2}$$

Equation (1) was used for load case i), while Equation (2) was used for load case ii). Specifically, the latter load case was limited by the yield strength, because this misuse corresponds to a low life cycle fatigue condition.

2.2.2. Road Simulator Testing

The road simulator test was conducted on an MTS 329 4DOF bench at Streparava Testing Center (MTS Systems Corporation, Eden Prairie, MN, USA). The cross beam was assembled with a complete suspension system and fixed to a chassis frame. These elements constitute the entire system necessary

for both replicating the boundary conditions and the constraints present on the vehicle, and for reproducing the loads generated by wheels' movements on the cross beam. The Wheel Force Transducers (WFT) connected the wheel hub with the actuators.

The time histories used were derived from a tracking activity carried out on paths typical for this class of vehicle; the signal was processed by means of Multiple Purpose Testware series 793 from MTS. Thus, the forces at wheel used during the testing were related to the actual loads acting on the component throughout its lifespan. The mission tested was 250,000 km long, composed of four typical test paths (highway, urban, hill and rough terrain) and special racetrack events (steering and brakes). The test duration was about 650 h.

During the test, the shock absorbers were cooled by a water jacket (water temperature range 18–20 °C). Rubber parts (bushings and bumpers) were cooled through a compressed air system. When required by the program, the brake was activated by pneumatic oil unit equipped with an electric operation.

As previously stated, numerical analyses of the outputs of test benches have rarely been performed for suspension assemblies. To overcome these limits, a structured approach was developed for the present research.

Strain gauges were introduced corresponding to the component areas with the most relevant structural impact. This approach made it possible to measure data in the previously selected relevant zones in order to evaluate the test by means of a numerical output. The selection and installation of the strain gauges is related to the FEA outputs. For this particular case study, looking at the principal stress calculated from the FEA, it was verified that in the areas with the greatest stress, one component of the stress was predominant, while the others could be neglected. For this reason, linear strain gauges were installed in the most stressed areas (see Figure 5); the direction was set according to the relative orientation of the vectors identified by the plot of the main stress obtained from the FEA results. Specifically, here, the orientation of the vectors was the same for the different load cases analysed. The definition of the orientation for strain gauge number 1 based on the vector plot of the principal stresses is shown in Figure 6 as an example.

Hooke's Law (Equation (3)) was used to thoroughly transform the strains (ε) registered by the strain gauges into stresses (σ), accordingly to the guidelines for the elaboration of linear strain gauge results contained in [26].

$$\sigma = E\varepsilon \qquad (3)$$

Young's Modulus *E* was calculated based on the tensile tests of samples machined out of components close to the positions of the strain gauges. Specifically, during the previous characterization of the prototypes, it was found that samples extracted from different areas had different mechanical properties (about 20 MPa in yield strength), which is mainly attributable to their dissimilar solidification speeds. More details regarding these tests can be found in a previous work by the authors [7]. The strain gauge areas (points from 1 to 6), along with the locations of the tensile specimens used for mechanical characterization, are presented in Figure 5. In particular, strain gauges from 1 to 4 were used for the road simulator test, while strain gauges 5 and 6 were used for the hydraulic steering system test. From each component, 4 "A" and "B" and 2 "M" samples were machined at symmetrical positions.
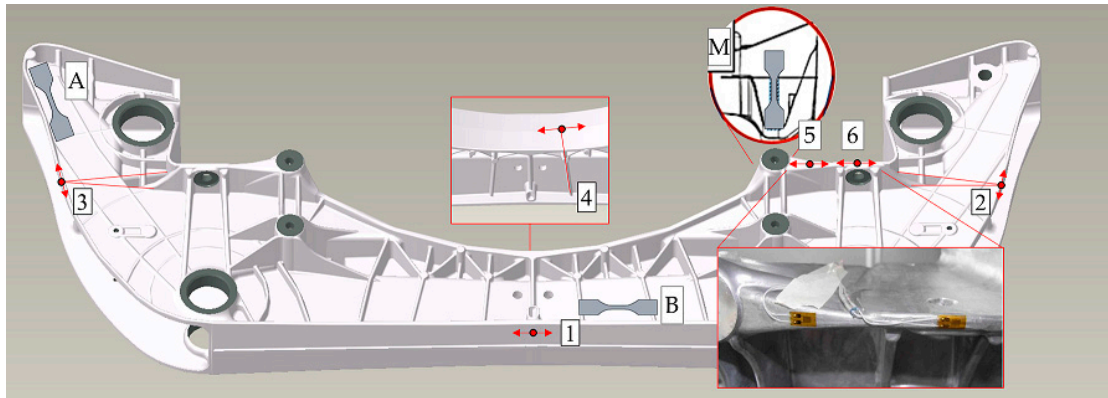
Figure 5. Strain gauge locations (numbers from 1 to 6) and tensile specimen positions (A, B, M).
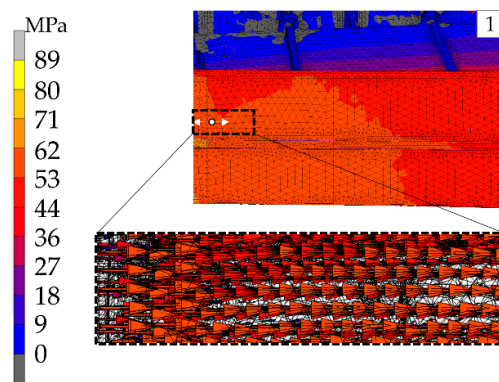

Figure 6. Strain gauge number 1 orientation based on principal stress vector plot of vertical load case.

It can be noted that strain gauges 2 and 3 are close to the "A" samples, while strain gauges 1 and 4 are closer to the "B" area. Thus, Young's Modulus (Equation (3)) was set to E_A = 74,980 MPa strain gauges 2 and 3 and E_B = 76,180 MPa strain gauges 1 and 4.

In the present work, the load cases traditionally used for suspension design, and which were considered during the previous dimensioning of the cross beam under study (reported in Section 2.2.1), are compared with the loads calculated based on time histories of actual track data, which will be used for the road simulator testing activity. Subsequently, the outputs of both the testing and FEA stresses will be compared.

2.2.3. Fatigue Testing of Cross Beam Resistance under Hydraulic Steering System Load

As already described in Section 2.2.1, the steering of a stationary vehicle generates relevant loads that act on the cross beam. This event cannot be evaluated during road simulator testing, thus necessitating a specific test bench.

This validation was conducted on a computer-controlled electrohydraulic servo system MTS test bench with equipment that was fit to purpose at the Streparava Testing Center, as outlined in Figure 7. The test bench was composed of: i) MTS 244 hydraulic actuator, ii) Linear Variable Differential Transducer (LVDT), iii) load cell and tools specifically designed and built in-house at Streparava Testing Center in order to clamp the cross beam and apply the hydraulic steering system load.

The test was carried out under cyclic loads with the same maximum value employed for the simulations ($F_{1,2}$ = ± 29.5 kN), and lasted 8000 cycles. The loads were applied at the location corresponding to point "P", as represented in Figure 7.
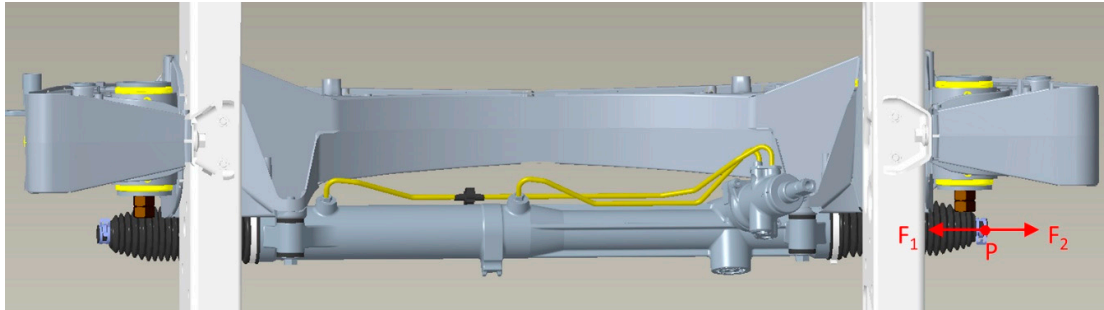
Figure 7. Configurations for the fatigue testing of cross beam resistance under hydraulic steering system load.

During the test, two strain gauges were introduced, corresponding to the component areas "5" and "6", as represented in Figure 5. The strain outputs were elaborated using Equation (3), in the same way as already reported in the "road simulator testing" section. Young's Modulus $E_M = 74{,}600$ MPa was derived on the basis of tensile tests of samples machined out from position M (as shown in Figure 5).

For the sake of clarity, this misuse load case corresponds to the steering of a stationary vehicle, and thus, it is independent from the vehicle path, in contrast to the other load cases. This is why this simpler load set used during experimental testing is equal to the one simulated. Thus, Section 3 does not report a comparison between the FEA and the testing inputs, and focuses only on the stress output evaluations.

2.2.4. FEA and Testing Correlation

The correlation method for comparing FEA and testing presented here is based on:

i)   Identification of the testing load inputs (real data based on WTF acquisition) with all three components (*Fx*, *Fy*, *Fz*) as close as possible to those of the FEA load cases,
ii) Micro-strain acquisition with strain gauges located in regions identified based on the evaluation of FEA results,
iii) Calculation of testing stresses using empirical Young's modulus and Hooke's law.

It is worthwhile noting that, if verified, this three-step method could be systematically implemented during the analysis of other complex systems in order to validate innovative projects in a reliable and verifiable way; it is not limited to suspension assemblies.

2.2.5. End-of-Testing Observations: Liquid Penetrant Testing and Microstructure

Following the endurance tests, the component was analysed through liquid penetrant testing to ensure no crack propagation had occurred during the experiments.

The casting surfaces were also observed using Optical Microscopy (OM) Leica DMI 5000M (Leica Microsystem, Milan, Italy), and Scanning Electron Microscopy (SEM) LEO EVO 40 (Zeiss, Milan, Italy). Semi-quantitative chemical analyses were carried out by means of an Energy Dispersive Spectroscopy (EDS) Link Analytical eXL probe (Oxford Instruments, Milan, Italy), with a spatial resolution of a few microns.

3. Results and Discussion

3.1. FEA Results

The general behavior of the component was analysed, looking firstly at the Von Mises stresses, which helped to locate the most stressed areas. Figure 8 reports the Von Mises stresses for the four conditions applied in the MSC Marc/Mentat finite element model under the different load conditions already described. Specifically, three conditions were obtained from the road input data elaborated

with MSC/Adams (vertical, brake, lateral), while one condition was related to the relevant interactions with the hydraulic steering system. The threshold considered for the output analysis corresponds to the permissible stress of the component, which was already reported in Section 2.2.1. The blue-colored areas correspond to low stress, while the red and yellow ones indicate increasing solicitations.
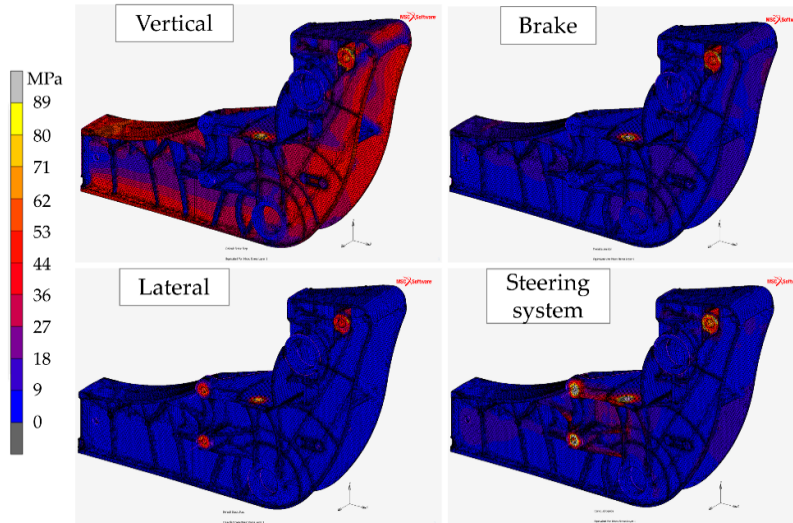

Figure 8. MSC Marc/Mentat Von Mises output for vertical, brake, lateral and hydraulic steering system load cases.

On the basis of the analysis of Figure 8, it can be noted that the mechanical stresses are generally comprised below the threshold, except for some spots that are slightly above the limit (yellow-colored areas). These regions contain the connections of the cross beam to the shock absorber, to the frame and to the hydraulic steering system. The stresses are located in small areas, and they are mainly related to compression stresses of about 100 MPa, always below the yield strength. It is worthwhile noting that the presence of these local peaks could derive from the presence of rigid links representing the nut-screw during the simulation of the connection areas. In terms of the response of the cross beam under different load cases, the forces in the vertical direction provide the greatest overall stresses, while the steering load case gives the highest local mechanical solicitation (~100 MPa local peak). For a more extensive evaluation of the tensile and compression zones, Figure 9 reports the principal stresses in the most stressed areas.

It is important to highlight that the overall stresses are below the threshold. The fulfilment of the resistance limits is an excellent result for this kind of component. Indeed, as stated previously, cross beams for CV are typically made of heavy metals due to the elevated mission loads related to this class of vehicle. To the of the authors' knowledge, the component developed during the present project is the first example of an aluminium cross member for CV. The structural resistance, preliminarily demonstrated by FEA results, is also related to the specific design of the component achieved after a careful iteration activity [7], leading to the final hollowed shape studied in this paper.

Another purpose of the structural simulation was determining the critical points at which to bond the strain gauges. These were located in the areas that showed the highest overall stresses. At the same time, to reduce the error of the measurements, the strain gauges were installed in areas not affected by assembly procedures and that had surfaces that were as planar as possible. This last point is a relevant item to reduce the discrepancy of results during the correlation activity.

The location of the strain gauges for the road simulator and hydraulic steering system tests are shown in Figure 5. In addition, Figure 9 focuses on the structural response that led to the selection of these areas. The stresses forecast in these zones will be used for the correlation of each load case with the laboratory tests results. The red and yellow areas indicate increasing solicitations, while the blue-colored ones correspond to low or compression stresses.
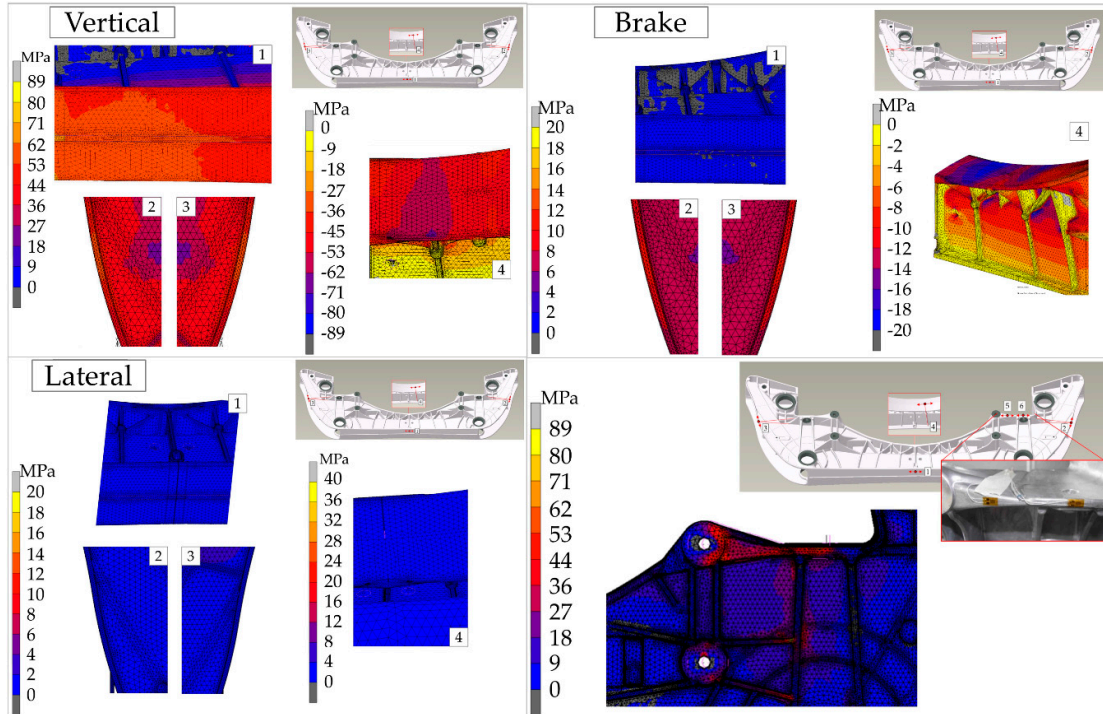
Figure 9. MSC Marc/Mentat principal stress outputs, focusing on the strain gauges areas.

3.2. Road Simulator Testing

Figure 10 displays some examples of the loads at wheel (a) and stress values from the strain gauges output (b) for the principal missions (rough terrain, highway urban) performed during the road simulator test. "L WFT" and "R WFT" are left and right wheel force transducer loads, "ER #" identifies the strain gauge number. For the purpose of a better understanding, a focus on a section of the mission is reported in Figures 11–13 for rough terrain, highway and urban time histories respectively.
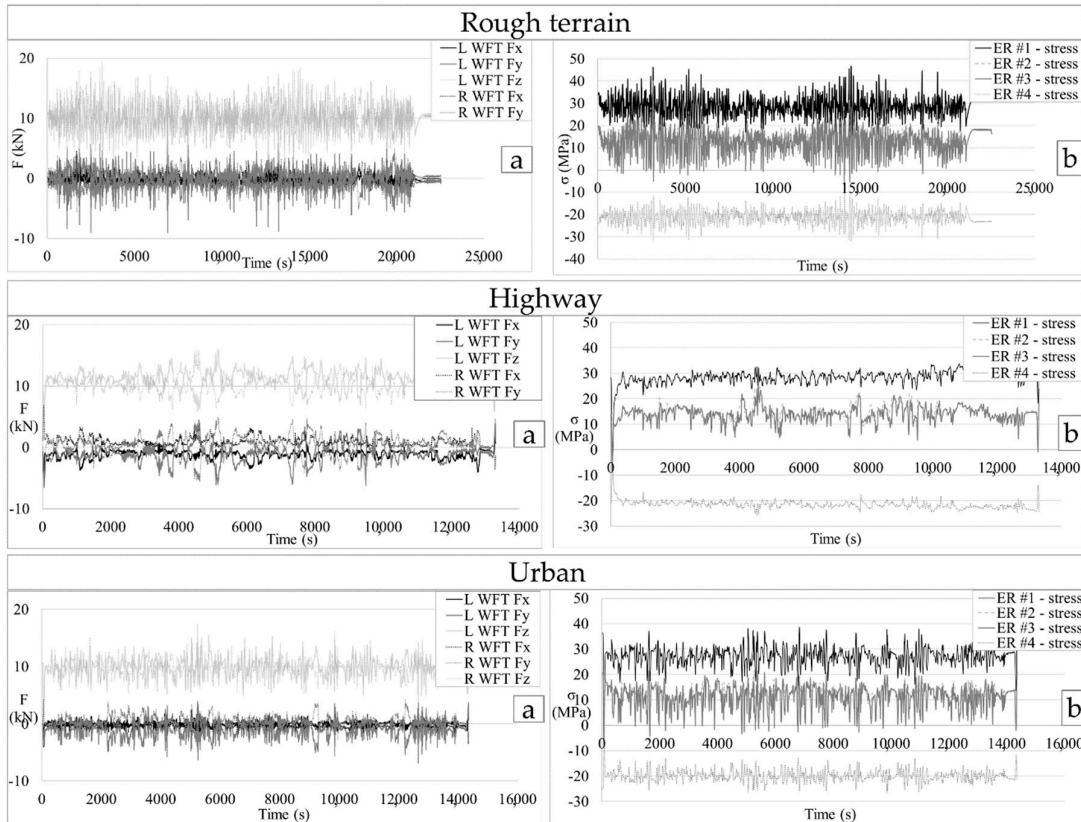
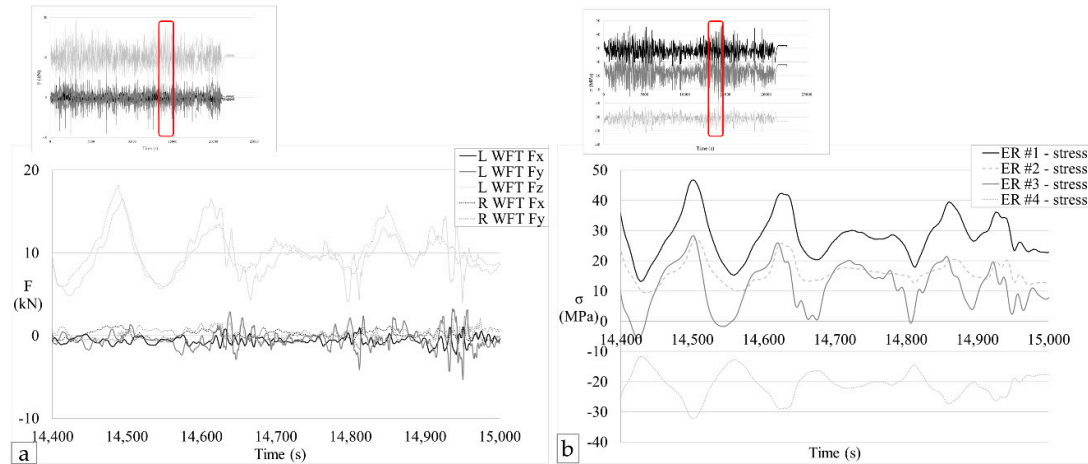**Figure 10.** Load at wheel (**a**) and strain gauge outputs (**b**) for the rough terrain, highway and urban missions.

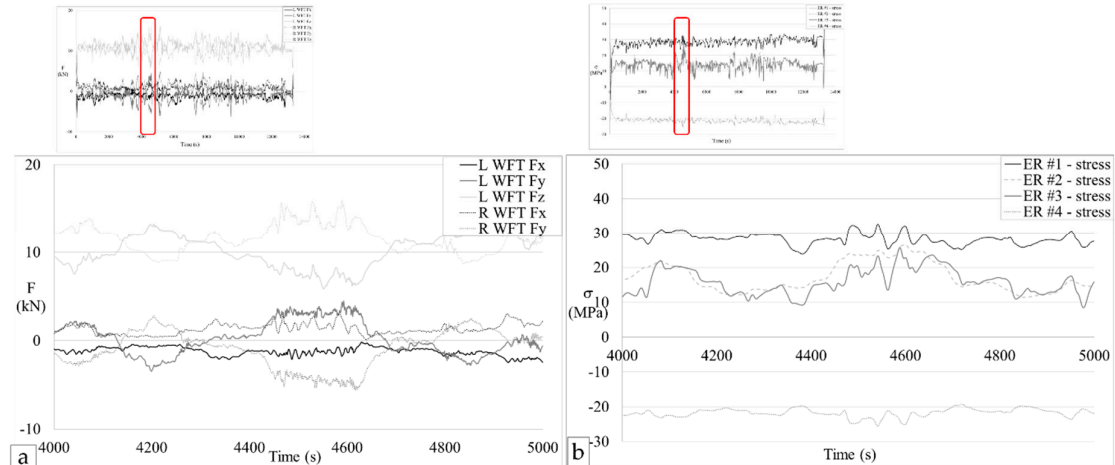**Figure 11.** Time frame of load at wheel (**a**) and strain gauge outputs (**b**) for the rough terrain mission.

Figure 12. Time frame of load at wheel (**a**) and strain guage outputs (**b**) for the highway mission.
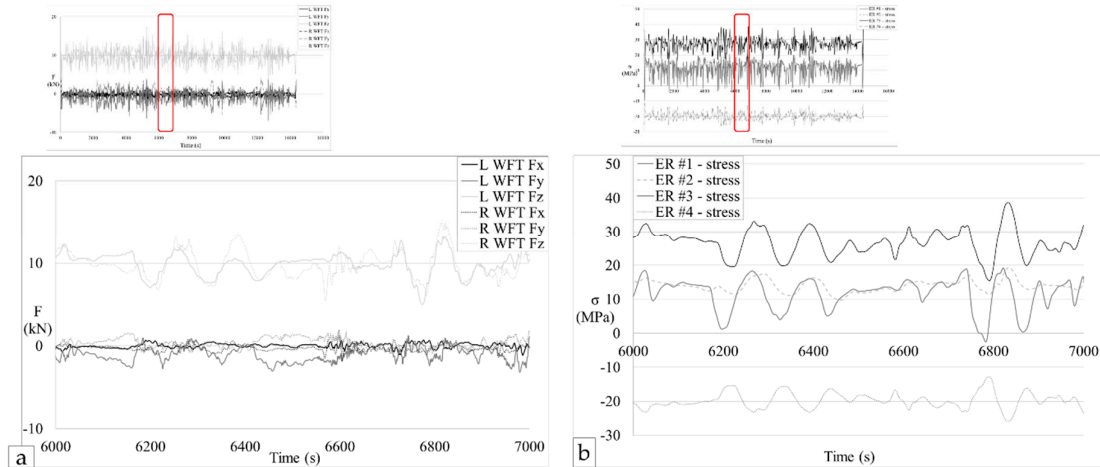

Figure 13. Time frame of load at wheel (**a**) and strain gauge outputs (**b**) for the urban mission.

Based on the analysis of these diagrams, it can be seen that the stress values (maximum peaks ~50 MPa) were lower than the fatigue limit of aluminum EN-AC 43,500 (σ_{FAF} = 89 MPa [25], as reported in Section 2.1). Thus, for the life time of the component, no fatigue damage is expected.

The highest stress peaks were registered during the rough terrain track, as expected from the input loads, and in correspondence with strain gauge #1. In addition, the symmetry between strain gauge #1 (tension stresses) and strain gauge #4 (compression stresses) was confirmed.

The road simulator test of the cross beam was successfully completed. Indeed, during the 250,000 km test, there was no evidence of events that might compromise the integrity of the component. The final analysis reported in Section 3.4 confirmed this statement.

Since MBS was conducted with different single load sets (see Section 2.2.1), while road simulator testing was based on time histories (see Section 2.2.2), the first necessary activity is to compare the input loads. The main purpose of this is to confirm the reliability of traditional MBS load cases by evaluating their magnitude in comparison with time histories that had been derived on the basis of real tracking activity. The results obtained from MBS were traditionally evaluated in terms of maximum stresses; thus, the peak loads were used as the basis of comparison: the maximum value of each load direction (F_x, F_y, F_z) of the time histories was identified and matched with the most similar MBS load case.

Table 3 reports the MBS load cases and the corresponding peak loads of the missions identified on the basis of the comparison explained above. It can be noted that the maximum loads were similar

between simulation and testing, with values being slightly higher for the former. Thus, the reliability of the traditional load cases was confirmed, also guaranteeing a safety margin for the dimensioning of the studied component.

Table 3. Load cases applied in MSC/AdamsCar (MBS) and the time histories of peak loads.

	F_X (kN)	F_Y (kN)	F_Z (kN)
MBS: load case "Vertical"	0	0	24.7
Road simulator: mission "rough-terrain"	−1.47	−2.46	19.20
MBS: load case "Brake"	−14.19	0	15.7
Road simulator: mission "special racetrack - brake"	−10.70	0.34	15.22
MBS: Load case "Lateral"	0	−14.5	20.6
Road simulator: mission "special racetrack - steering"	−2.06	−12.90	14.13

Subsequently, testing load inputs with all three components (F_x, F_y, F_z) as close as possible to the MBS load cases were identified. This step is necessary in order to find the mission that best fits each loading set, based on a combination of the three most similar loading components, and to consequently guarantee the most reliable correlation possible between the MSB and testing outputs. Table 4 reports the set of testing input forces closest to the MBS ones.

Table 4. Input for each load case applied in MSC/AdamsCar (Multibody Simulation MBS) and the related road simulator time histories.

	Left WFT			Right WFT		
	F_X	F_Y	F_Z	F_X	F_Y	F_Z
MBS: Load case "Vertical"	0	0	24.7	0	0	24.7
Road simulator: mission "rough-terrain"	−0.71	−0.55	15.30	1.00	−0.11	18.10
MBS: Load case "Brake"	−14.19	0	15.7	14.2	0	15.17
Road simulator: mission "special racetrack - brake"	−7.72	−0.96	12.49	7.68	1.04	12.13
MBS: Load case "Lateral"	0	−14.5	20.6	0	0	0
Road simulator: mission "special racetrack - steering"	−1.62	−12.26	15.54	−0.61	4.11	3.84

The outputs corresponding to these input conditions were registered for each load case, both for the road simulator and MBS, as reported in Table 5. In particular, the output values reported for the MBS are based on Figure 9.

Table 5. Output stresses from MSC/AdamsCar (Multibody Simulation MBS) and the related road simulator time histories.

	ER #1	ER #2	ER #3	ER #4
Load case "Vertical"	54.5	53.0	53.0	−60.5
Road simulator: mission "rough-terrain"	46.7	27.1	28.0	−32.1
Load case "Brake"	0.0	8.0	14.0	−20.0
Road simulator: mission "special racetrack - brake"	20.2	11.5	12.3	−21.8
Load case "Lateral"	0.0	0.0	0.0	0.0
Road simulator: mission "special racetrack - steering"	19.7	7.4	9.3	−16.9

Based on the analysis of Table 5, the accuracy of the finite element simulation can be confirmed. Indeed, the average discrepancy of the simulated and testing stress outputs is limited to about 14 MPa, which is in agreement with the few similar works that could be retrieved from literature [27,28]. In addition, the stresses registered and calculated are always below the permissible stress condition reported in Equation (1) (89 MPa), confirming the reliability of the dimensioning condition with respect to the actual component behaviour. It is worthwhile noting that even if the input testing load sets selected are the closest to the MBS dimensioning forces, they still slightly differ each other. The limited discrepancy of the stress output is also related to this input difference. Finally, it is worthwhile noting that there are several conditions similar to those reported in the table that satisfy this correspondence, due to the cyclic nature of the test, as can be appreciated by looking at the WFT to time diagrams reported in Section 3.2.

3.3. Fatigue Testing of Cross Beam Resistance under Hydraulic Steering System Loads

The minimum and maximum stresses registered during the test were from −30 MPa to 25 MPa and from −9 MPa to 4 MPa for strain gauges #5 and #6, respectively.

The test was successfully completed, as concluded from both the low stress values acting on the component and the absence of events that might damage the component during the experiments.

Table 6 reports the stresses measured in the strain gauge positions ER#5 and ER#6 during the test, compared with those calculated on the basis of the "hydraulic steering system" load case. Specifically, the output values reported for the simulation are related to those reported in Figure 9.

Table 6. Stress calculated on the basis of MSC/AdamsCar and measured based on the hydraulic steering system testing.

				ER #5	ER #6
			load case "hydraulic steering system"	30	15
	+F_1 29		Fatigue testing bench "hydraulic steering system"	25	4
Input loads (kN)		Output stresses (MPa)	load case "hydraulic steering system"	−30	−15
	−F_1 −29		Fatigue testing bench "hydraulic steering system"	−30	−9

Conclusions similar to those reported in Section 3.2 for MBS and road simulator testing correlation could be reached. It can be noted that the numerical and experimental stress outputs were very similar, with an average difference of about 6 MPa. This discrepancy is lower than in the road simulator case, due to both the equivalence of the loads used as the input for testing and simulation

and also to the simpler features of the system tested. Indeed, this test bench was composed of the cross beam and the hydraulic steering system, while the road simulator test bench comprised the entire suspension assembly, the complexity of which could contribute to generating some additional dissimilarities.

3.4. End-of-Testing Observations: Liquid Penetrant Testing and Microstructure

Figure 14 shows the results of the liquid penetrant inspection carried out on samples following the road simulator and hydraulic steering system test benches. A single discontinuity was detected, and this is reported in the upper-right part of Figure 14. The defect was investigated in detail in order to determine its nature by means of optical and SEM analysis on sections transversal to the cross beam (Figure 15a and 15b, respectively). The direction of the section is indicated by a dotted line and two arrows on the upper right side of Figure 14.
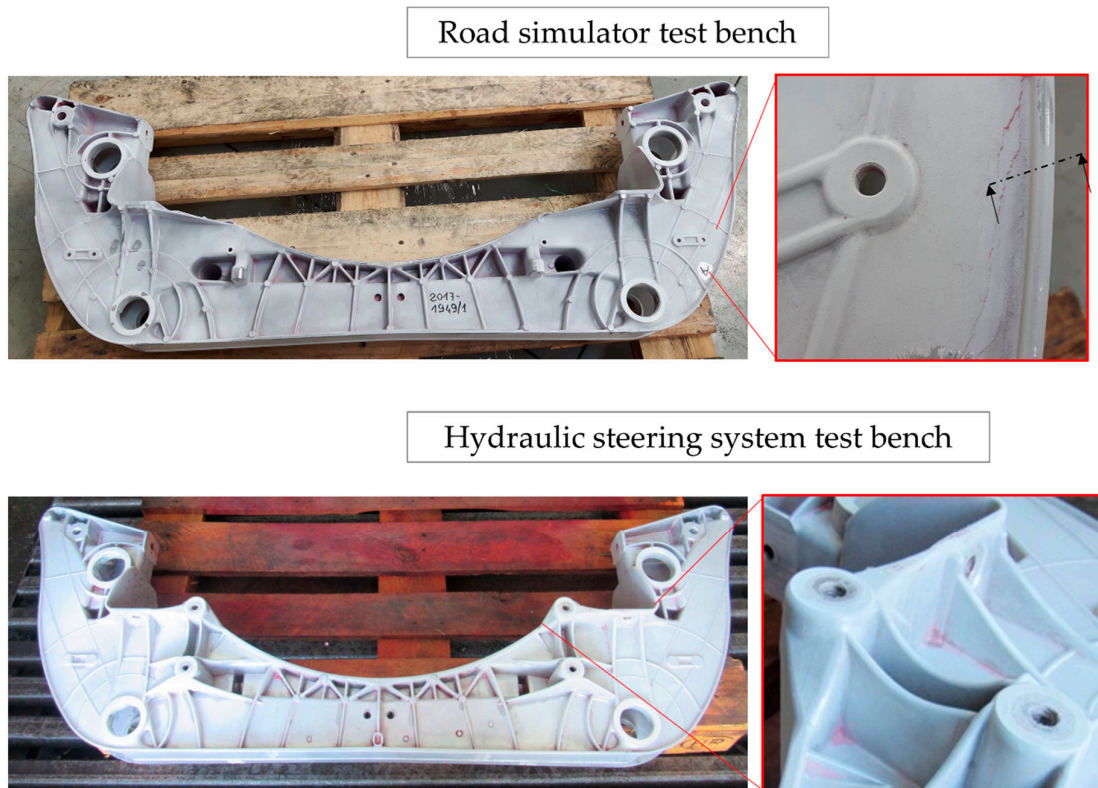

Figure 14. Liquid penetrant testing on cross beam after the road simulator and hydraulic steering system test benches. Arrows indicate the metallographic sections.
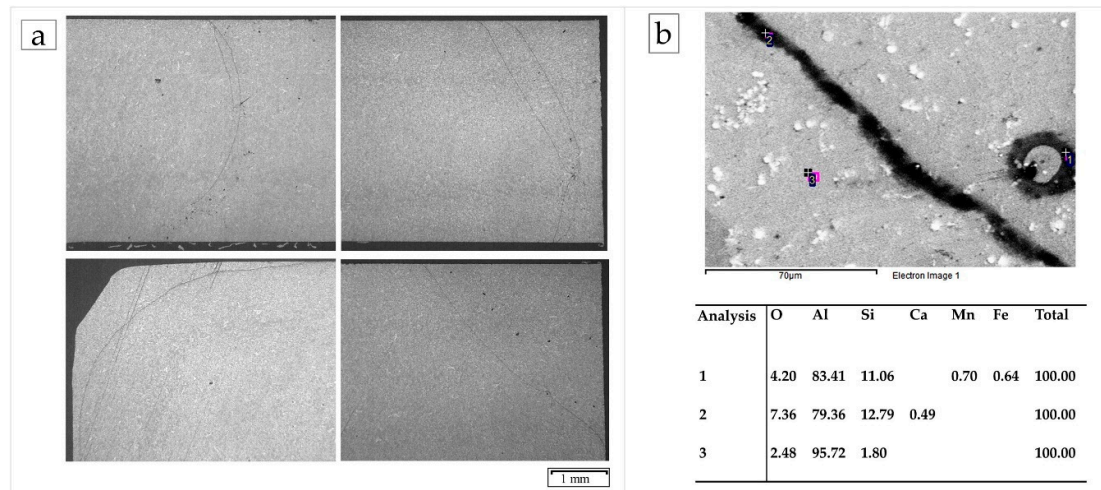
Figure 15. (**a**) Optical micrographs of defects revealed by liquid penetrant testing; (**b**) SEM observation with EDS analysis of this defect.

The analysis revealed that the discontinuity detected was related to a foundry defect, usually referred to as lamination. Lamination is one of the most common surface defects in die casting, and forms when a relatively warm metal vein at low viscosity flows between the steel die and partially solidified metal [29]. In the specific case studied, the defect is located next to two ejector pins acting on a cross beam wall that remained unrestrained following slider extraction. An additional factor affecting defect inception is that, at this stage of the HPDC process, it is possible that the aluminium casting is not yet completely solidified, due both to the elevated dimensions of the components and to the high process speed.

The EDS analysis reported in Figure 15b shows that the lamination consists mainly of eutectic Al-Si phase (analysis #1 and #2). This is in agreement with the previous hypothesis since, as is well known, the onset of the eutectic formation of Al-Si alloys takes place at lower temperatures (and solidifies at a later casting stage) than the pre-eutectic aluminium matrix (analysis #3) [30]. Thus, during component extraction, the ejector pins cause the lamination of the component, which is immediately penetrated by the eutectic, which is still a liquid at this stage. Then, the eutectic solidification fills this gap and the laminated areas merged together to create a sound section. Indeed, the microstructures reported in Figure 15 confirm that the eutectic area is coherent with the remaining section, and no cracks were detected in the different sections. It is important to highlight that the microstructure corresponds to a typical EN AC-43500 microstructure, composed of α-Al matrix with Al-Si globular modified eutectic in the interdendritic space and some intermetallic compounds.

It is worth noting that the presence of this defect was also verified in other components that had not been subjected to the road simulator test. Indeed, real components always have defects of varying natures (shrinkage porosities, air entrapped, oxides, lamination, etc.), especially for parts with such high dimensions. The safety of the designed components is guaranteed by the introduction of a safety coefficient accounts for the eventual presence of defects. With regard to the road simulator test, the time histories employed represent the heaviest missions that could be found for real vehicle use, while also containing some misuse conditions, in order to additionally ensure the safety of the final application. The testing of real components with some defects typical of the production process is a further verification of the effectiveness of the safety coefficient used during the design process. The successful testing of this kind of component is even more relevant than on the testing of a completely sound one.

For the particular case studied, the absence of cracks even after the endurance tests further confirms the coherency of the solidified eutectic with the remaining aluminium matrix. The

successful result of the testing indicates that this kind of defect does not invalidate component resistance, and thus the component is acceptable for application.

Finally, it can be concluded that this modified cross beam structure of an independent front suspension can endure a 250,000 km road mission, applied without fatigue failure.

4. Conclusions

The present paper introduced a method for deeply investigating the structural resistance of new components. The model was applied to an innovative lightweight cross beam, the features of which had been specifically selected (design, alloy, process, etc.) both to reduce the weight and to be able to resist the elevated mission loads.

In particular, FEA simulations and fatigue test benches were employed to evaluate the resistance under different conditions representative of operating environments. Then, the data obtained from the test benches were numerically elaborated in order to compare them with the analytical results. Real data from in-field measurements was used to provide results that could increase the confidence levels for this new application.

The main results can be summarized as follows:

FEA

- The mechanical solicitations were generally below the safety threshold for all load cases analysed, which confirms the resistance of the innovative re-designed aluminium at the elevated operation loads.
- Some local compressive peaks (maximum stress ~100 MPa) were observed corresponding to the following cross beam interfaces: shock absorber, frame and hydraulic steering system. Note that the values calculated in these areas could be affected by the presence of rigid links used for the simulation of the connection.
- The greatest overall stresses were obtained for the vertical load case, while the highest local mechanical solicitation (~100 MPa local peak) was caused by the steering system forces.

Test benches

- The 250,000 km road simulator test bench was successfully completed. The stress values measured (maximum peaks ~50 MPa) were always lower than the fatigue limit (σ_{FAF} = 89 MPa).
- The testing of the hydraulic steering system was successfully completed. The higher loads registered were ~30 MPa, with similar values for tension and compression state.

FEA and testing correlation

- The reliability of the traditional load cases used during FEA was confirmed. Indeed, the maximum loads used during the road simulator test were comparable to the simulated ones. It was also confirmed that FEA guarantees a safety margin, since these loads were slightly higher than the values calculated on the basis of in-field acquisition.
- The FEA and testing results were aligned. The average discrepancies were limited to only about 14 MPa and 6 MPa for the road simulator test bench and the hydraulic steering system test, respectively. The difference registered was lower for the latter experiment due to the simpler structure of this test bench.

Finally, it can be concluded that:

- The demonstration of the fulfilment of the resistance limits is an excellent result for this kind of component. Indeed, it was verified that the hollowed shape of the innovative cross beam endured at the elevated mission loads typical for this class of vehicle. These results can also be extended to the redesign of other safety-relevant components belonging to this class of vehicle.
- The correlation method presented in this paper was proven to be reliable, since it enabled not only the numerical evaluation of the testing output, but also the validation of the

calculation tools. The three-step method presented in this paper could be systematically applied for the analysis of other complex systems, not limited to suspension assemblies, in order to validate innovative projects in a reliable and verifiable way. It is worthwhile to remember that a rigorous evaluation of the results is a relevant item for safety-critical components.

Author Contributions: Conceptualization, S.C. and D.F.; Data curation, S.C., F.M. and G.C.; Formal analysis, S.C., and G.C.; Investigation, S C.; Methodology, S.C. and F.M.; Project administration, D.F.; Software, D.F. and F.M.; Supervision, D.F. and G.C.; Validation, D.F.; Visualization, G.C.; Writing – original draft, S.C.; Writing – review & editing, F.M. and S.C.

Conflicts of Interest: The authors declare no conflict of interest.

References

1. Helms, H.; Lambrecht, U. The potential contribution of light-weighting to reduce transport energy consumption. *Int. J. Life Cycle Assess.* **2007**, *12*, 58–64.
2. Modaresi, R.; Pauliuk, S.; Lovik, A.N.; Muller, D.B. Global carbon benefits of material substitution in passenger cars until 2050 and the impact on the steel and aluminum industries. *Environ. Sci. Technol.* **2014**, *48*, 10776–10784.
3. Das, S. Life Cycle Energy and Environmental Assessment of Aluminum-Intensive Vehicle Design. *SAE Int. J. Mater. Manuf.* **2014**, *7*, 588–595.
4. Bertram, M.; Buxmann, K.; Furrer, P. Analysis of greenhouse gas emissions related to aluminium transport applications. *Int. J. Life Cycle Assess.* **2009**, *14*, 62–69.
5. Dioni, D.; Cecchel, S.; Cornacchia, G.; Faccoli, M.; Panvini, A. Effects of artificial aging conditions on mechanical properties of gravity cast B356 aluminum alloy. *Trans. Nonferrous Met. Soc. China* **2015**, *25*, 1035–1042.
6. Cecchel, S.; Chindamo, D.; Turrini, E.; Carnevale, C.; Cornacchia, G.; Gadola, M.; Panvini, A.; Volta, M.; Ferrario, D.; Golimbioschi, R. Impact of reduced mass of light commercial vehicles on fuel consumption, CO_2 emissions, air quality, and socio-economic costs. *Sci. Total Environ.* **2018**, *613–614*, 409–417, doi:10.1016/j.scitotenv.2017.09.081.
7. Cecchel, S.; Ferrario, D.; Panvini, A.; Cornacchia, G. Lightweight of a cross beam for commercial vehicles: Development, testing and validation. *Mater. Des.* **2018**, *149*, 122–134, doi:10.1016/j.matdes.2018.04.021.
8. Chindamo, D.; Gadola, M. Reproduction of real-world road profiles on a four-poster rig for indoor vehicle chassis and suspension durability testing. *Adv. Mech. Eng.* **2017**, *9*, 1–10, doi:10.1177/1687814017726004.
9. Chindamo, D.; Lenzo, B.; Gadola, M. On the vehicle sideslip angle estimation: A literature review of methods, models and innovations. *Appl. Sci.* **2018**, *8*, 355, doi:10.3390/app8030355.
10. Azrulhisham, E.A.; Asri, Y.M.; Dzuraidah, A.W.; Nik Abdullah, N.M.; Shahrum, A.; Che Hassan, C.H. Evaluation of Fatigue Life Reliability of Steering Knuckle Using Pearson Parametric Distribution Model. *Int. J. Qual. Stat. Reliab.* **2010**, *8*, doi:10.1155/2010/816407.
11. Lee, D.C.; Han, C.S. CAE (Computer Aided Engineering) driven durability model verification for the automotive structure development. *Finite Elem. Anal. Des.* **2009**, *45*, 324–332, doi:10.1016/j.finel.2008.10.004.
12. Bladh, K. Virtual Full Vehicle Durability Testing of a Coach. Master's Science Thesis MMK 2012:17 MKN 055. KTH Industrial Engineering and Management, Stockholm, Sweden, 2012.
13. Dressler, K.; Speckert, M.; Bitsch, G. Virtual durability test rigs for automotive engineering. *Veh. Syst. Dyn.* **2009**, *47*, 387–401, doi:10.1080/00423110802056255.
14. Magalhaes, R.R.; Fontes, C.H.; Vieira de Melo, S.A.B. Failure analysis and design of a front bumper using finite element method along with durability and rig tests. *Int. J. Veh. Des.* **2012**, 71–83, https://doi.org/10.1504/IJVD.2012.049158.
15. Uberti, S.; Gadola, M.; Chindamo, D.; Romano, M.; Galli, F. Design of a double wishbone front suspension for an orchard/vineyard tractor: A kinematic analysis. *J. Terramech.* **2015**, *57*, 23–39.

16. Mattetti, M.; Molari, G.; Vertua, A. New methodology for accelerating the four-post testing of tractors using wheel hub displacements. *Biosyst. Eng.* **2015**, *129*, 307–314.

17. Cecchel, S.; Collotta, M.; Cornacchia, G.; Panvini, A.; Tomasoni, G. A comparative cradle-to gate impact assessment: Primary and secondary aluminum automotive components case. *La Metall. Ital.* **2018**, *2*, 46–55.

18. Cecchel, S.; Cornacchia, G.; Panvini, A. Cradle-to-Gate Impact Assessment of a High-Pressure Die-Casting Safety-Relevant Automotive Component. *JOM* **2016**, *8*, 2443–2448, doi:10.1007/s11837-016-2046-3.

19. Cecchel, S.; Cornacchia, G.; Gelfi, M. Corrosion behavior of primary and secondary AlSi High Pressure Die Casting alloys. *Mater. Corros.* **2017**, *68*, 961–969, doi:10.1002/maco.201709526.

20. Cecchel, S.; Chindamo, D.; Collotta, M.; Cornacchia, G.; Panvini, A.; Tomasoni, G.; Gadola, M. Lightweighting in light commercial vehicles: Cradle-to-grave life cycle assessment of a safety relevant component. *IJLCA* **2018**, 1–12, doi:10.1007/s11367-017-1433-5.

21. Cornacchia, G.; Cecchel, S.; Panvini, A. A comparative study of mechanical properties of metal inert gas (MIG)-cold metal transfer (CMT) and fiber laser-MIG hybrid welds for 6005A T6 extruded sheet. *Int. J. Adv. Manuf. Technol.* **2017**, *94*, 2017–2030.

22. Cecchel, S.; Ferrario, D. Numerical and experimental analysis of a high pressure die casting Aluminum suspension cross beam for light commercial vehicles. *La Metall. Ital.* **2016**, *6*, 41–44.

23. Cecchel, S.; Cornacchia, G.; Gelfi, M. A study of a non-conventional evaluation of results from salt spray test of aluminum High Pressure Die Casting alloys for automotive components. *Mater. Corros.* **2019**, *70*, 70–78, doi:10.1002/maco.201810307.

24. Cecchel, S.; Cornacchia, G.; Panvini, A. Low temperature T6 heat treatment of AlSi9Cu3(Fe) high pressure die casting actual automotive components. *J. Mater. Eng. Perform.* **2018**, *27*, 3791, doi:10.1007/s11665-018-3478-4.

25. Primary aluminium alloys for pressure die casting Available online: http://rheinfelden-alloys.eu/wp-content/uploads/2016/01/05-HB-DG_Ci_Sf_Cm_Td_Ma_RHEINFELDEN-ALLOYS_2015_EN.pdf (accessed on 1 August 2019).

26. Uni ente italiano di normazione. *UNI 10478-4:1998, Prove non Distruttive-Controllo Mediante Estensimetri Elettrici a Resistenza-Circuiti di Misura, Elaborazione e Presentazione dei Risultati*; Uni ente Italiano di Normazione: Milano, Italy, 1998.

27. Dong, Z.; Wang, X.; Lou, W.; Huang, Y.; Zhong, M.; Fan, H.; Peng, L. Simulation of the Spindle Coupled Multi-Axial Loading Fatigue Test of a Minivan Rear Axle. *Strength Mater.* **2017**, *49*, 872–896, doi:10.1007/s11223-018-9933-5.

28. Palma, E.S.; Dos Santos, E.S. Fatigue damage analysis in an automobile stabilizer bar. *Proc. Inst. Mech. Eng. Part D J. Automob. Eng.* **2002**, *216*, 865–871, doi:10.1243/095440702321031414.

29. Casari, D.; Merlin, M.; Garagnani, G.L. Influence of injection parameters on the final surface quality of Al-Si-Cu die cast components. *Metall. Sci. Technol.* **2012**, *30*, 12–18.

30. Canalesa, A.A.; Talamantes-Silva, J.; Gloria, D.; Valtierra, S.; Colás, R. Thermal analysis during solidification of cast Al–Si alloys. *Thermochim. Acta* **2010**, *510*, 82–87, doi:10.1016/j.tca.2010.06.026.